

# Journal of Materials Chemistry B

Accepted Manuscript



This is an *Accepted Manuscript*, which has been through the Royal Society of Chemistry peer review process and has been accepted for publication.

*Accepted Manuscripts* are published online shortly after acceptance, before technical editing, formatting and proof reading. Using this free service, authors can make their results available to the community, in citable form, before we publish the edited article. We will replace this *Accepted Manuscript* with the edited and formatted *Advance Article* as soon as it is available.

You can find more information about *Accepted Manuscripts* in the [Information for Authors](#).

Please note that technical editing may introduce minor changes to the text and/or graphics, which may alter content. The journal's standard [Terms & Conditions](#) and the [Ethical guidelines](#) still apply. In no event shall the Royal Society of Chemistry be held responsible for any errors or omissions in this *Accepted Manuscript* or any consequences arising from the use of any information it contains.

# Self-Assembling Doxorubicin-Prodrug Nanoparticles as siRNA Drug Delivery System for Cancer Treatment: *In Vitro* and *In Vivo*

Hongmei Liu,<sup>ab</sup> Chenmeng Qiao,<sup>c</sup> Jun Yang,<sup>a</sup> Jie Weng<sup>\*c</sup> and Xin Zhang <sup>\*a</sup>

<sup>a</sup> National Key Laboratory of Biochemical Engineering, Institute of Process Engineering, Chinese Academy of Sciences, Beijing, 100190, PR China. Tel: +86 010 82544853; Fax: +86 010 82544853; E-mail address: xzhang@home.ipe.ac.cn

<sup>b</sup> University of Chinese Academy of Sciences, Beijing, 100049, PR China

<sup>c</sup> Key Laboratory of Advanced Technologies of Materials, School of Materials Science and Engineering, Southwest Jiaotong University, Chengdu, Sichuan, 610031, PR China, Tel: +86 28 87601371; Fax: +86 28 87601371; E-mail address: jweng@swjtu.edu.cn

## Abstract

Co-delivery of siRNAs and chemotherapeutic drugs to kill tumor have achieved superior tumor growth inhibition. However, due to siRNAs and chemotherapeutic drugs with different molecular properties, co-delivery carriers use more cationic materials to bind siRNAs and excessive inert materials to embed drugs, causing low drug loading contents and the systemic toxicity. To achieve this goal, doxorubicin (DOX) is chemically conjugated to stearyl chloride (C18) through N-Methyldiethanol amine (N) as crosslinker to form amphiphilic C18-N-DOX. C18-N-DOX contains a tertiary amine, which can complex siRNAs at low pH (pH 3) and reduce the density of the positive charges on the surface of NPs at physiological pH (pH 7.4). C18-N-DOX together with 1, 2-distearoyl-sn-glycero-3-phosphoethanolamine-N-methoxy-poly (ethylene glycol 2000) DSPE-PEG2000 self-assemble into DOX-prodrug nanoparticles (DOX-prodrug NPs), which bind siRNAs in citrate buffer (pH 3) to form DOX-prodrug NPs/siRNA. After citrate buffer (pH 3) replacing with PBS (pH 7.4), DOX-prodrug NPs/siRNA have slight

negative charges, due to complexed more siRNAs. In this study, clear evidence is showed that DOX-prodrug NPs can deliver siRNA to the same tumor cells both *in vitro* and *in vivo*. Meanwhile, DOX-prodrug NPs/siRNA show a great effect on inhibiting tumor cell growth both *in vitro* and *in vivo*. Therefore, the DOX-prodrug NPs are promising candidates as siRNAs delivery system for tumor therapy.

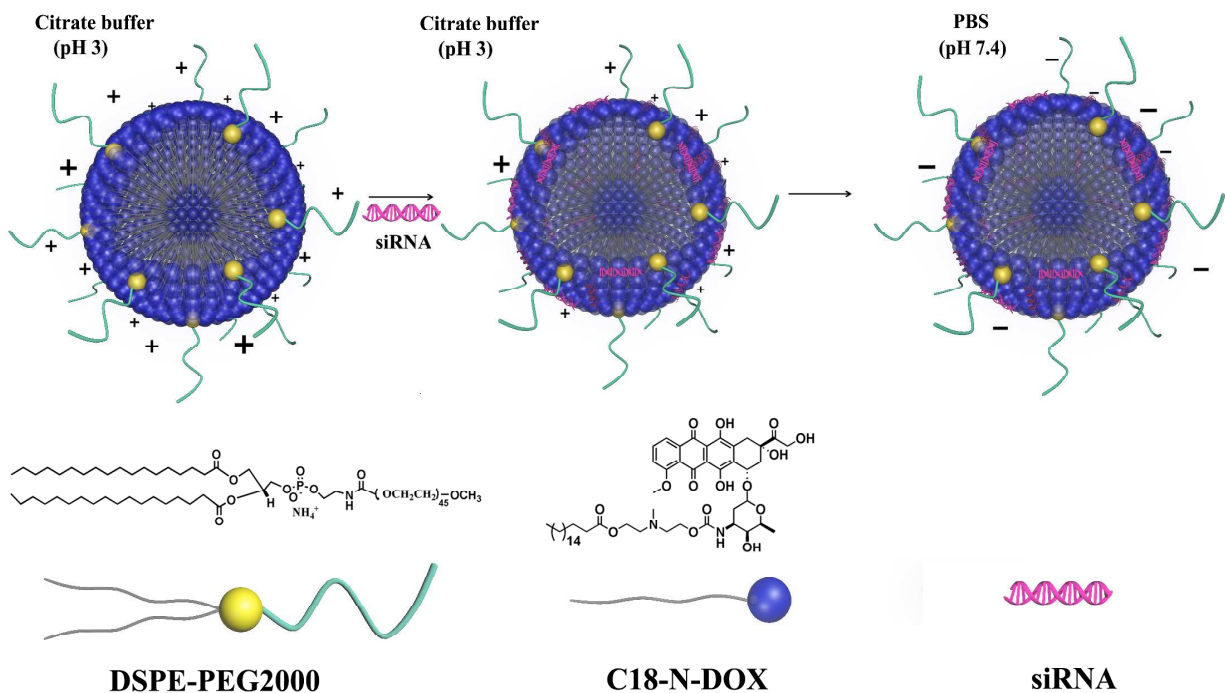
## Introduction

The death rate from cancer continues to increase and is one of the leading causes of death in the world.<sup>1</sup> Co-delivery two different drugs with different anticancer mechanisms to target cancer cells, especially co-delivery of nucleic acid and chemotherapeutic drugs has attracted more attention and achieved better effect.<sup>2-5</sup> To enable the therapeutic use of siRNAs and anticancer drugs, an effective siRNAs and anticancer drugs co-delivery system is required. Many researches about nanocarriers using anticancer drugs and siRNAs co-delivery to inhibit the growth of tumors were highlighted recently, and had made great progresses on therapeutic applications.<sup>6-10</sup> The co-delivery platforms should be designed to overcome hurdles such as enzymatic degradation, negatively charges and large size of siRNAs and the side effects of chemotherapy drugs. To achieve these goals, nanoparticle platforms composed of different materials with different features provided advantages for siRNAs and chemotherapy drugs co-delivery. Such drug co-delivery systems based on polymers,<sup>11</sup> liposomes<sup>12</sup> or inorganic materials<sup>13</sup> always used more positive charge materials to bind siRNAs and excessive inert materials to embed drugs. However, the introduction of too many carriers results in low drug-loading content and increases the metabolic burden and systemic toxicity.<sup>14</sup>

DOX as a most widely used anticancer drug is crucial to the treatment of various type of cancers such as breast, ovarian, cervical and gastric cancers and so on.<sup>15,16</sup> DOX causes DNA

damage and induction of apoptosis through the inhibition the progression of the enzyme topoisomerase II.<sup>17</sup> Small interfering RNA (siRNA) can selectively hybridize with target mRNA and degrade the complementary target mRNA in a sequence-specific manner at a post-transcriptional level.<sup>18,19</sup> Combination of two or more therapeutic drugs with different mechanisms can effectively inhibit tumor growth. Currently, many researchers have developed the most effective carriers for co-delivery of DOX and a therapeutic siRNA to inhibit tumor growth.<sup>20-23</sup> However, the DOX loading efficiency was very low and loading content of DOX in previous studies was generally not greater than 15%.<sup>24,25</sup>

Herein, we have successfully developed DOX-prodrug NPs for siRNA delivery for overcoming the above-mentioned siRNA and drug delivery difficulties (Scheme 1). DOX was chemically conjugated to stearoyl chloride (C18) through N-Methyldiethanol amine (N) as crosslinker to form amphiphilic C18-N-DOX. The C18-N-DOX self-assembled into DOX-prodrug NPs when stabilized with DSPE-PEG2000. These DOX-prodrug NPs were designed on the basis of the following reasons: (i) tertiary amines with positive charge density are highly pH dependent, in pH 3 with high cationic charge can bind siRNA and in pH 7.4 can reduce the positive charge density on the surface of NPs,<sup>26-30</sup> (ii) reduce the amount of inert materials to embed DOX and enhance the DOX loading efficiency, due to conjugated anticancer compound. These features made DOX-prodrug NPs an excellent carrier for delivery of siRNA for cancer therapy. In this study, the ability of DOX-prodrug NPs to deliver siRNA into the same tumor cells was examined both *in vitro* and *in vivo*. We provided clear evidence that DOX-prodrug NPs co-delivery of chemotherapeutic drugs and anticancer siRNAs cooperatively inhibited the tumor growth in a combined manner.



**Scheme 1.** Structural composition of DOX-prodrug NPs with DSPE-PEG2000 and C18-N-DOX. The DOX-prodrug NPs can complex siRNA in pH 3 citrate buffer. After replacing pH 3 citrate buffer with pH 7.4 PBS, the DOX-prodrug NPs/siRNA have slight negative charges on the surface of NPs.

## Experimental Section

### Materials

N-Methyldiethanol amine was purchased from Aladdin Co. Ltd., China. Pyridine was purchased from Alfa Aesar. DOX·HCl was obtained from Dalian Meilun Biotech Co. Ltd., (Dalian, China). Di (N-succinimidyl) Carbonate (DSC) and Stearoyl Chloride were got from TCI (Japan). Glo Lysis buffer and steady-Glo® Luciferase Assay System were obtained from promega. 1, 2-distearoyl-sn-glycero-3-phosphoethanolamine-N-methoxy-poly (ethylene glycol 2000) (DSPE-PEG2000) was obtained from Shanghai Advanced Vehicle Technology Ltd. Co. Antibodies against human polo-like kinase 1 (Plk1) and  $\beta$ -actin were obtained from Santa cruz

Biotechnology. Goat anti-mouse IgG-HRP antibody, goat anti-rabbit IgG (H+L), BCA Protein Assay Kit, Bradford Protein Assay and lysis buffer (RIPA) were purchased from Beyotime (China). siRNAs targeting human Plk1 (siPlk1) (sense strand, 5'-UGAAGAAGAUCACCCUCCUAdTdT-3'; antisense strand, 5'-UAAGGAGGGUGAUCUUCUUCAdTdT-3') and scrambled siRNA (siNonsense) (sense strand, 5'-UUCUCCGAACGUGUCACGudTdT-3'; antisense strand, 5'-ACGUGACACGUUCGGAGAAAdTdT-3'), Luc-siRNA: sense: (5'-CCCUAUUCUCCUUCUUCGCdTdT -3', antisense: 5'-GCGAAGAAGGAGAAUAGGGdTdT -3'); Cy5-labeled siRNA: (sense strand: 5'-Cy5-CCUUGAGGCAUACUUCAAAAdTdT-3', antisense strand: 5'-UUUGAAGUAUGCCUCAAGGdTdT -3') were supplied by Su Zhou Ribo Life Science Co. Ltd. (Suzhou, China). In situ cell death detection kit, POD was obtained from Roche (Mannheim, Germany). 3-(4, 5)-dimethyl-2-thiazolyl)-2, 5- diphenyltetrazolium Bromide (MTT) and 4', 6-Diamidino-2-phenylindole Dihydrochloride (DAPI Dihydrochloride) were got from TCI Shanghai. Dichloromethane was dry by calcium hydride.

## Methods

### Synthesis of C18-N-OH Conjugates

N-Methyldiethanol amine (20 mL) and 98 mmol of pyridine were dissolved in anhydrous CH<sub>2</sub>Cl<sub>2</sub>. 4.88 g (40 mmol) stearoyl chloride was dissolved in 20 mL of anhydrous CH<sub>2</sub>Cl<sub>2</sub> and was added in a drop-wise manner into the N-Methyldiethanol amine and pyridine mixture solution at 0 °C. The reaction was carried out for 3 h at room temperature. The resultant solution was diluted by dichloromethane and washed with brine solution for three times. Subsequently, the resultant solution was dried over anhydrous Na<sub>2</sub>SO<sub>4</sub>. The organic phase was collected and dried under vacuum after removing the solvent with a yield of 83%. <sup>1</sup>H NMR (600 MHz, CDCl<sub>3</sub>

$\delta$  ppm) was carried out to characterize the C18-N-OH:  $\delta$  4.18 (O=C-O-CH<sub>2</sub>-CH<sub>2</sub>, t,  $J$  = 5.7 Hz, 2H), 3.63 – 3.56 (HO-CH<sub>2</sub>-CH<sub>2</sub>, m, 2H), 2.71 (N-CH<sub>2</sub>-CH<sub>2</sub>, t,  $J$  = 5.7 Hz, 2H), 2.62 – 2.59 (N-CH<sub>2</sub>-CH<sub>2</sub>, m, 2H), 2.36 – 2.29 (CH<sub>3</sub>-N&O-CO-CH<sub>2</sub>, m, 5H), 1.66 – 1.58 (CH<sub>2</sub>-CH<sub>2</sub>-CH<sub>2</sub>, m, 2H), 1.32 – 1.24 (CH<sub>2</sub>-CH<sub>2</sub>-CH<sub>2</sub>, m, 28H), 0.89 (CH<sub>2</sub>-CH<sub>3</sub>, t,  $J$  = 7.0 Hz, 3H).

### Synthesis of C18-N-DOX Prodrugs

C18-N-OH (2 g, 5.2 mmol) was reacted with DSC (2.22 g, 8.7 mmol), which was dissolved in 20 mL of dichloromethane. The reaction was carried out for 6 h at room temperature. By precipitation in ice-chilled n-hexane, the resulting C18-N-DSC was retrieved with a yield of 75%. Further reactions were carried out by reacted C18-N-DSC (184 mg, 0.35 mmol) with 200 mg (0.35 mmol) of DOX which dissolved in anhydrous dimethyl formamide (DMF) in the presence triethylamine (1.05 mmol). The reaction was allowed to proceed for 48 h under nitrogen atmosphere. The crude product was purified by column chromatography on silica gel (200-300 mesh) eluted with 0-10% methanol gradient in dichloromethane. <sup>1</sup>H NMR (600 MHz, DMSO-*d*<sub>6</sub>  $\delta$  ppm) was carried out to characterize the C18-N-DOX:  $\delta$  14.05 (HO-Ph, s, 1H), 13.29 (HO-Ph, s, 1H), 7.92 (H-Ph, d,  $J$  = 4.1 Hz, 2H), 7.69 – 7.64 (H-Ph, m, 1H), 6.66 (-OCNH-, d,  $J$  = 7.9 Hz, 1H), 5.45 (OH, s, 1H), 5.22 (-CH(O)<sub>2</sub>, d,  $J$  = 3.1 Hz, 1H), 4.96 (Ph-CH-O, d,  $J$  = 4.0 Hz, 1H), 4.84 (OH, t,  $J$  = 6.0 Hz, 1H), 4.67 (OH, d,  $J$  = 5.6 Hz, 1H), 4.57 (O=C-CH-O, d,  $J$  = 6.0 Hz, 2H), 4.15 (Me-CH-O, q,  $J$  = 6.3 Hz, 1H), 4.04 (O=C-O-CH<sub>2</sub>-CH<sub>2</sub>, t,  $J$  = 5.6 Hz, 2H), 3.99 (CH<sub>3</sub>O-, s, 3H), 3.92 (HO-CH<sub>2</sub>-CH<sub>2</sub>, m, 2H), 3.69 (O=C-NH-CHC<sub>2</sub>, d,  $J$  = 4.9 Hz, 1H), 3.44 (HO-CHC<sub>2</sub>, d,  $J$  = 3.7 Hz, 1H), 2.98 (Ph-CH<sub>2</sub>-C, s, 2H), 2.63 – 2.52 (N-CH<sub>2</sub>-CH<sub>2</sub>, m, 4H), 2.30 – 2.11 (CH-CH<sub>2</sub>-C&CH<sub>3</sub>-N&O-CO-CH<sub>2</sub>, m, 7H), 1.83 (C-CH<sub>2</sub>-C, td,  $J$  = 12.8, 3.6 Hz, 1H), 1.48 (C-CH<sub>2</sub>-C, m, 3H), 1.23 (C-CH<sub>2</sub>-C, m, 28H), 1.13 (CH<sub>3</sub>-C, d,  $J$  = 6.5 Hz, 3H), 0.85 (CH<sub>2</sub>-CH<sub>3</sub>, dd,  $J$  = 7.0 Hz, 3H). The mass and molecular formula of C18-N-DOX were determined by

Fourier Transform Ion Cyclotron Resonance Mass Spectrometer (positive, Bruker, USA)  $m/z$  955.51  $[M + H]^+$ , calcd for  $C_{51}H_{74}N_2O_{15}$ , 954.51; found, 954.51 (Fig. S1).

### **DOX-Prodrug NPs/siRNA Complexes Formulation**

DOX-prodrug NPs/siRNA complexes formulations were prepared as previously described method.<sup>31</sup> C18-N-DOX and DSPE-PEG2000 were completely solubilized in ethanol at a molar ratio of 7:1. The C18-N-DOX and DSPE-PEG2000 mixture was added to an aqueous buffer (100 mM citrate, pH 3) with mixing to final ethanol and lipid concentrations of 35% (v/v) and 3 mg  $mL^{-1}$ , respectively. The siRNA (solubilized in a 100 mM citrate, pH 3, 35% ethanol) was added to the empty NPs. After a NPs/siRNA weight ratio of 21:1 was achieved, the mixture was incubated for 3 min at 55 °C to allow NPs reorganization and encapsulation of the siRNA. The ethanol was then removed, and the external buffer was replaced with PBS (pH 7.4) by dialysis using a 10,000 molecular weight cutoff membrane.

### **Size, Zeta Potential and Colloidal Stability Measurements**

Particle size and zeta potential were determined using a Malvern Zetasizer NanoZS. Colloidal stability was measured by incubating DOX-prodrug NPs/siRNA in Dulbecco's Modified Eagle Medium (DMEM) with high glucose supplemented with 10% fetal bovine serum (FBS) at 37 °C under gentle stirring. At each time point, the mean diameters of hybrid NPs were monitored by using DLS.

### **The Morphology of DOX-Prodrug NPs**

The morphology of DOX-prodrug NPs was observed by transmission electron microscopy (TEM) (H-7650 TEM, Japan). These NPs were dripped on to 200 mesh copper grids coated with carbon and were dyed with 2% phosphotungstic acid. To further ascertain the structure of DOX-



prodrug NPs, cryo-transmission electron microscopy (FEI Tecnai 20 Cryo-TEM) was used to take images of NPs in a frozen state.

### **DOX, DOX-N-C18 and DOX-prodrug NPs loading into siRNA.**

DOX and DOX-N-C18 (1.5  $\mu\text{M}$ ) were prepared by incubating siRNA with the increasing molar ratios. The DOX-prodrug NPs were prepared in pH 7.4 PBS by incubating siRNA with the increasing molar ratios. The fluorescence spectra of DOX were scanned at an excitation wavelength of 480 nm by a microplate reader (Infinite M200 PRO, Tecan).

### **DOX Equivalent Loading and *In Vitro* Release of DOX from DOX-Prodrug NPs**

The loading efficiency (LE) was determined as the amount of DOX equivalents in the DOX-prodrug NPs.<sup>32</sup>

$$\text{LE} = \frac{\text{Amount of DOX equivalents in NPs}}{\text{Amount of C18 - N - DOX} + \text{Amount of DSPE - PEG2000}}$$

The release profiles of DOX from DOX-prodrug NPs were studied using a dialysis tube (MWCO 10,000) under shaking (200 rpm) at 37 °C in PBS (pH 7.4). The equivalent concentration of DOX 3 mg mL<sup>-1</sup>, 1 mL DOX-prodrug NPs was dialyzed against 25 mL of release media. At desired time intervals, 1 mL release media was taken out and replenished with an equal volume of fresh media. The amount of DOX released was determined by using a microplate reader (SpectraMax M5, Molecular Devices, CA) with excitation at 470 nm and emission at 590 nm.

### **Preparation of DOX-Prodrug NPs/siRNA and Gel Retardation Assay**

To test the binding ability of DOX-prodrug NPs, the gel electrophoresis was carried out. Gel electrophoresis was performed using 2% (w/v) agarose gel in TEA buffer with 0.5  $\mu\text{g mL}^{-1}$  of EtBr. DOX-prodrug NPs complexed with siRNA at NPs/siRNA weight ratios 7:1, 21:1, 28:1, 35:1 and 50:1 in citrate buffer (pH 3) and in PBS (pH 7.4), respectively, were prepared for

electrophoresis. The electrophoretic mobility of DOX-prodrug NPs/siRNA was visualized on a UV transilluminator at an excitation wavelength of 302 nm. The gel electrophoresis was applied for 10 min (100 V/cm).

### **Cell Culture**

The *HeLa* cells and *HeLa*-Luci cells were maintained in DMEM with high glucose supplemented with 10% FBS and 1% v/v penicillin/streptomycin at 37 °C with 5% CO<sub>2</sub>.

### **Cellular DOX Uptake and Intracellular Release of DOX**

The cellular uptake of DOX-prodrug NPs was tested by BD FACS Calibur flow cytometer and intracellular release behaviors of DOX-prodrug NPs were followed with CLSM using *HeLa* cells. The cells were cultured in a 24-well plate and were incubated with DOX-prodrug NPs for 2 h, cells were washed twice with PBS, digested with trypsin solution, and analyzed on a BD Calibur (BD Bio. sciences USA).

The cells were cultured on microscope slides using DMEM supplemented with 10% FBS. The cells were incubated with DOX-loaded micelles for 2 or 24 h at 37 °C. The culture medium was removed and the cells were rinsed three times with PBS. The fluorescence images were obtained using CLSM (Japan, Nikon).

### ***In Vitro* Analysis of DOX-Prodrug NPs Delivery siRNA into Tumor Cells**

DOX-prodrug NPs containing Cy5-labeled siRNA was prepared as described above. *HeLa* cells ( $4 \times 10^4$  cells/well) were seeded in a 24-well culture plate. The DOX-prodrug NPs/Cy5-siRNA solution was incubated with *HeLa* cells for 2 h. After 2 h incubation, cells were washed three times with PBS, lysed with trypsin and analyzed on a BD FACS Calibur flow cytometer (BD Biosciences, USA).

For CLSM observations, *HeLa* cells ( $4 \times 10^4$  cells/well) were seeded in a 35 mm glass bottom culture dish and incubated for 24 h at 37 °C in 5% CO<sub>2</sub>, allowed to grow until 50% confluent and followed by adding the DOX-prodrug NPs/Cy5-siRNA solution. After 2 h of incubation, the cells were washed with PBS for twice and the cells were visualized using A1RSi CLSM with a 60 × objective (Japan, Nikon).

### ***In Vitro* Gene Transfection and Analysis of Gene Expression**

*HeLa*-Luci cells were transfected with DOX-prodrug NPs/siLuc. *HeLa*-Luci cells were plated at a cell density of  $4 \times 10^4$  cells/well in 24-well culture plates and allowed to adhere overnight. siRNA targeting luciferase or nonsense siRNA was complexed with DOX-prodrug NPs at the weight ratio of 1:21. Cells were incubated with DOX-prodrug NPs/siLuc for 12 h, after which the DOX-prodrug NPs/siLuc solutions were removed and replaced with fresh complete media. The luciferase assay was assessed after another 12 h post transfection using Centro XS<sup>3</sup> LB 960 Microplate Luminometer (Berthold technologies, Germany). The cells were washed with PBS and were digested by Glo lysis buffer for five minutes. 100 μL of medium was added into 96-well plates and mixed 100 μL of steady-Glo<sup>®</sup> reagent, then measured luminescence in a luminometer.

*HeLa* cells transfected with DOX-prodrug NPs/siPlk1. *HeLa* cells were plated at a cell density of  $4 \times 10^4$  cells/well in 12-well culture plates and allowed to adhere overnight. siPlk1 or nonsense siRNA was complexed with DOX-prodrug NPs at the weight ratio of 1:21. The *HeLa* cells were transfected with PBS, free siPlk1, DOX-prodrug NPs/nonsense siRNA and DOX-prodrug NPs/siPlk1 for 12 h, and then the culture medium was replaced with fresh DMEM medium. After incubation for another 12 h at 37 °C, the mRNA levels of Plk1 were detected by quantitative real-time polymerase chain reaction (qRT-PCR).

qRT-PCR was performed as described previously.<sup>33</sup> Primers for Plk1 and GAPDH are as followed: Plk1-forward 5'-AGCCTGAGGCCCGATACTACCTAC-3', Plk1-reverse 5'-ATTAGGAGTCCCACACAGGGTCTTC-3'; GAPDH-forward : 5'-TTCACCACCATGGAGAAGGC-3', GAPDH-reverse 5'-GGCATGGACTGTGGTCATGA-3'. The mRNA level of Plk1 was normalized to GAPDH.

For Western blot analysis, the cells were lysed with 100  $\mu$ L of lysis buffer (RIPA) and the supernatant was collected by 4  $^{\circ}$ C centrifugation for 10 min at 12,000 g. The concentration of protein was measured using the BCA kit. Total 80  $\mu$ g proteins were loaded on 12% SDS-polyacrylamide gel electrophoresis (SDS-PAGE) and then transferred to acetic nitrocellulose membranes for 90 min (120 V). After sealing with 5% bovine serum albumin (BSA) in PBS with Tween-20 (PBST) for 1 h, the membranes were incubated with monoclonal antibodies against Plk1 overnight. After three times of washing, the membranes were incubated with goat antimouse IgG-HRP antibody for 1 h, and the bands were visualized by 3, 3'-diaminobenzidine tetrahydrochloride (DAB) staining (0.5 mg mL<sup>-1</sup> with 0.1% H<sub>2</sub>O<sub>2</sub>).

### ***In Vitro* Cytotoxicity.**

*In vitro* cytotoxicity study of free DOX, DOX-prodrug NPs, DOX-prodrug NPs/nonsense siRNA and DOX-prodrug NPs/siPlk1 was quantitatively measured by employing on *HeLa* cells. The cells were seeded in 96-well plate for 24 h and then the medium was changed with various concentrations of free DOX or DOX-loaded NPs (range from 0.1 to 10  $\mu$ g mL<sup>-1</sup> in culture medium). *In vitro* cell viability was determined using the 3-(4, 5-Dimethylthiazol-2-yl)-2, 5-diphenyltetrazolium bromide (MTT) assay. At designed time intervals, the medium was removed and the wells were washed two times with PBS. Subsequently, 20  $\mu$ L MTT was added to each well and incubated for 2 h. Then, medium was removed and 150  $\mu$ L of DMSO was added. The

absorbance was measured at 570 nm using a plate reader. The percentage of cell viability was determined by comparing cells treated with various NPs to the untreated control cells.

### **Mouse Tumor Models**

All protocols for this animal study were conformed the Guide for the Care and Use of Laboratory Animals. All procedures involving experimental animals were performed in accordance with protocols approved by the Committee for Animal Research of Peking University, China. *HeLa* ( $2 \times 10^6$ ) cells were subcutaneously injected into the armpit of the 5-week-old female BALB/c nude mice. Tumors were allowed to grow to a uniform volume ( $\sim 50 \text{ mm}^3$ ).

### ***In Vivo* Fluorescence Imaging and Drug Distribution in Tumor Tissues**

*HeLa*-bearing female mice were intravenously injected with PBS (pH 7.4) (200  $\mu\text{L}$ ), free Cy5-siRNA (1  $\text{mg kg}^{-1}$ ) and DOX-prodrug NPs/Cy5-siRNA (at Cy5-siRNA concentration of  $\text{mg kg}^{-1}$ , in PBS (pH 7.4)) through the tail vein. 12 hours later, the mice were sacrificed and tissues were harvested. The tissues were imaged by the Kodak *in vivo* imaging system. For CLSM analysis, the tumor tissues were collected and fixed in 4% paraformaldehyde, and then cross-sectioned using a vibration microtome. In order to stain cell nucleus, the sectioned tissues were incubated in DAPI (0.5  $\mu\text{g mL}^{-1}$ ) solution in saline for 0.5 h at room temperature. Confocal imaging of tumor tissues was performed using A1Rsi CLSM (Japan, Nikon) equipped with 40  $\times$  oil objective and filter sets (DAPI (Ex341/Em461), DOX (Ex480/Em580) and Cy5-siRNA (Ex649/Em680)).

### **Tissue Distribution**

Free DOX (at 4.1  $\text{mg kg}^{-1}$ , 200  $\mu\text{L}$ ), DOX-prodrug NPs and DOX-prodrug NPs/siPlk1 (at 4.1  $\text{mg kg}^{-1}$ , 200  $\mu\text{L}$ ) were intravenously injected to ICR mice via tail vein using a syringe. 12 hours after injection, the mice were sacrificed and the tissues were harvested. To determine the tissue

distributions of DOX-prodrug NPs and DOX-prodrug NPs/siPlk1, DOX fluorescence in the specimen was imaged by the Kodak *in vivo* imaging system with excitation at 470 nm and emission at 590 nm. Quantitative analysis for the tissue distribution of micelles was carried out using the Living Imaging Software.

### **Blood Pharmacokinetics**

To determine pharmacokinetics, either DOX·HCl (at 4.1 mg kg<sup>-1</sup>, 200 μL), DOX-prodrug NPs or DOX-prodrug NPs/siPlk1 (at 4.1 mg kg<sup>-1</sup>, 200 μL) was intravenously injected into ICR mice through the tail vein using a syringe.<sup>34</sup> A blood sample (20 μL) was collected from the tail vein at different time points post injection and mixed with K3-EDTA (0.5 μL, an anticoagulation agent). To extract DOX, acetone (60 μL) was added to the blood, vortexed, and then the solution was centrifuged (5,000 g, 10 min). The supernatant was collected and stored at -80 °C until the time of analysis. The solution was loaded onto 96-well plate in triplicate (50 μL per well). Fluorescence was measured using a microplate reader (SpectraMax M5, Molecular Devices, CA) with excitation at 470 nm and emission at 590 nm. A linear standard curve of DOX ranging 10 ~ 0.1 μg mL<sup>-1</sup> was created and used for measuring the concentration of DOX in blood. The dataset was analyzed by PKSolver software. The data of free DOX fit to a one-compartment and the data of DOX-prodrug NPs and DOX-prodrug NPs/siPlk1 fit noncompartment pharmacokinetic model. All data were expressed as mean ± SD. n = 4.

### **Antitumor Effects**

Anti-cancer effect of DOX or DOX-loaded NPs was evaluated by measuring the tumor volume in a double-blinded manner. After reaching a tumor volume by ~ 50 mm<sup>3</sup>, the tumor *HeLa*-bearing mice were randomized into five groups. The mice received PBS (200 μL), free DOX (4.1 mg kg<sup>-1</sup>, 200 μL), free siPlk1 (0.5 mg kg<sup>-1</sup>, 200 μL), DOX-prodrug NPs/nonsense siRNA (at 4.1

equivalent DOX mg kg<sup>-1</sup> and at 0.5 mg kg<sup>-1</sup> siRNA, 200 μL) and DOX-prodrug NPs/siPlk1 (at 4.1 equivalent DOX mg kg<sup>-1</sup> and at 0.5 mg kg<sup>-1</sup> siRNA, 200 μL) through tail vein injection at day 0, 2, 4 and 6 post initial treatment. Tumor size and body weight were measured. Tumor volume was measured as follows:

$$V = (a \times b^2) / 2$$

where a and b represent the major and minor axes of a tumor, respectively. The lengths of the axes were measured using a caliper. Tumor volume in each group was compared by relative tumor volume:<sup>35</sup>

Relative tumor volume = tumor volume/initial tumor volume before treatment

#### **Measurements of Plk1 Expression in Tumor Tissue**

Tumor tissues were collected 24 h after the last treatment, digested by an RNeasy mini kit. The level of Plk1 mRNA was analyzed by qRT-PCR as describe above. To determine the Plk1 protein expression in tumor tissue after treatments, tumor tissues were collected 24 h after the last injection. The tumor tissues were lysed and the total 80 μg protein was collected and analyzed by Western blot assay as described above.

#### ***In Vivo* TUNEL Assay**

The mice were sacrificed 18 days after the first injection, and tumor tissues were collected and fixed in 4% paraformaldehyde overnight at 4 °C. TUNEL assay was performed on the excised tumor tissues using in situ cell death detection kit, POD (Roche) according to the manufacturer's protocol. Tumor sections were transferred onto the glass slide and deparaffinized. 50 μL of proteinase K (50 μg mL<sup>-1</sup>) in TBS (pH 8.0) was added onto the slides and incubated for 30 min at room temperature. After rinsed with PBS for three times, the slides were incubated with TUNEL reaction mixtures for 60 min at 37 °C in a humidified atmosphere in the dark. The slides were

washed with PBS. The 50  $\mu\text{L}$  TUNEL reaction mixtures were mixed with 2  $\mu\text{L}$  enzyme solution and 48  $\mu\text{L}$  label solution. After rinsed with PBS for three times, the slides could be analyzed in a drop of PBS under CLSM by using 488 nm excitation and 530 nm emission at this state. The cells with green fluorescence were defined as apoptotic cells. DAPI was used to stain cell nucleus.

### **Cardiac Toxicity Study**

The heart tissues of each mouse were collected, fixed, and processed thereafter for H&E staining. Images of cardiac tissue sections were collected using a Nikon light microscope with 400  $\times$  magnification.

### **Statistical Analysis**

Statistical analysis was performed by using the Student's t-test with  $p < 0.05$  as significant difference. The experimental results were given in the format of mean, mean  $\pm$  SD in the figures.

## **Results and discussion**

### **Synthesis and Characterization of C18-N-DOX**

In the present work, we synthesized the C18-N-DOX. The chemical structure of C18-N-DOX was given in Fig. 1A. First, stearoyl chloride reacted with N-Methyldiethanol amine to form C18-N-OH. C18-N-OH was then coupled with DOX through DSC to form carbamate-linked C18-N-DOX. The formation of DOX, C18-N-OH or C18-N-DOX was first confirmed by  $^1\text{H-NMR}$  spectroscopy with all the characteristic peaks and the integration values of DOX, C18-N-OH and C18-N-DOX as indicated in Fig. 1B, C and D, respectively. The reaction at the  $\text{NH}_2$  group of DOX was confirmed by the appearance of NH at  $\delta$  6.67 ppm. Moreover, the proton at the 1 position of DOX shifted from  $\delta$  3.34 ppm to  $\delta$  3.70 ppm during the conjugation, indicating that the DOX and C18-N-DSC reaction has occurred. The resulting C18-N-DOX was further



examined by high resolution mass spectroscopy to determine its mass and molecular formula. As shown in Fig. S1, the result was consistent with the expected formula of the C18-N-DOX. The mass and molecular formula of C18-N-DOX were determined by Fourier Transform Ion Cyclotron Resonance Mass Spectrometer (positive, Bruker, USA)  $m/z$  955.51  $[M + H]^+$ , calcd for  $C_{51}H_{74}N_2O_{15}$ , 954.51; found: 954.51. These data indicated that C18-N-DOX was synthesized.

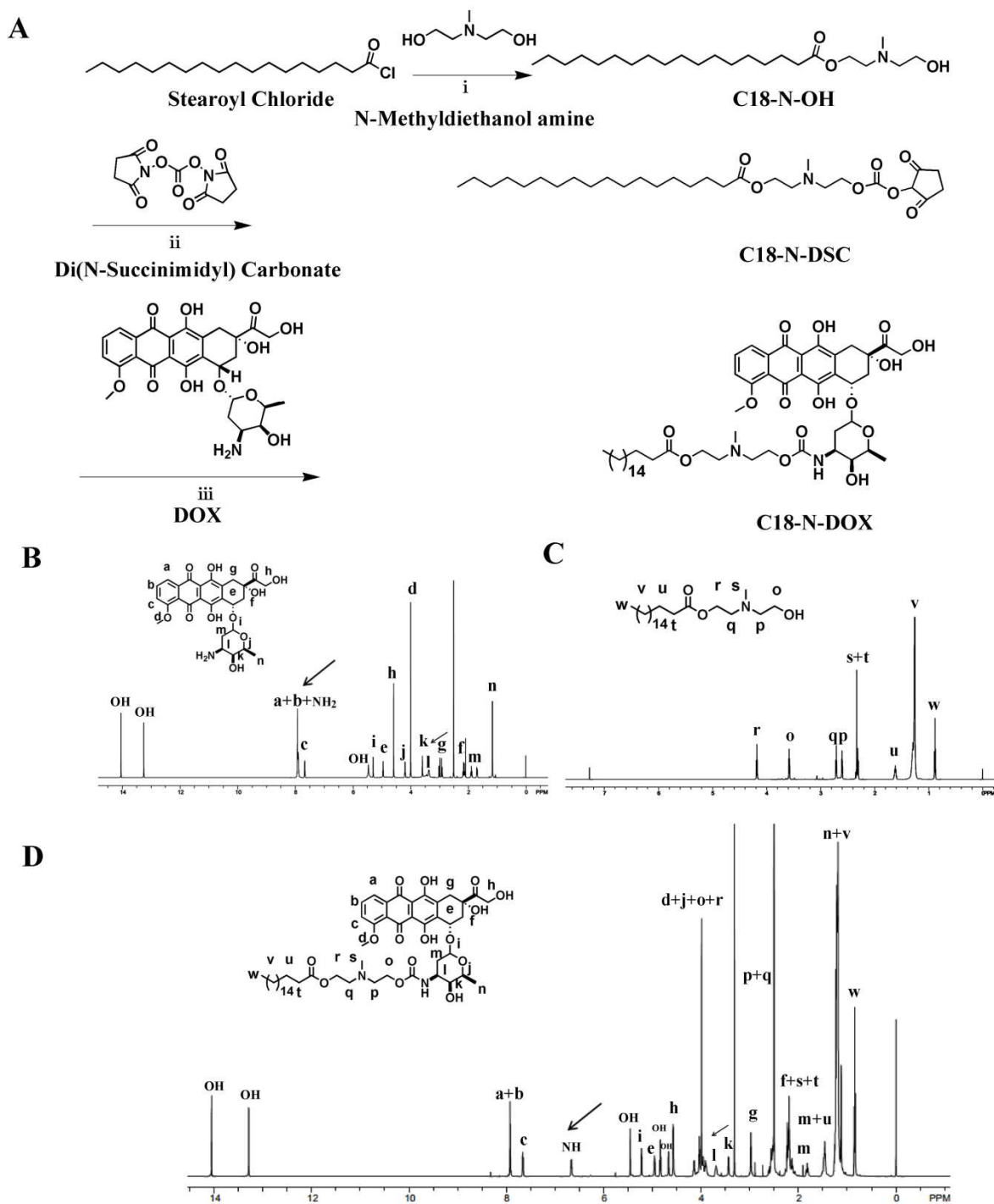


**Fig. 1** Synthesis and characterization of C18-N-DOX. A) Synthetic route of the C18-N-DOX. B)  $^1\text{H}$  NMR spectra of DOX (600 MHz,  $\text{DMSO-}d_6$ ). C)  $^1\text{H}$  NMR spectra of C18-N-OH (600 MHz,  $\text{CDCl}_3$ ). D)  $^1\text{H}$  NMR spectra of C18-N-DOX (600 MHz,  $\text{DMSO-}d_6$ ).

### Preparation and Characterization of DOX-prodrug NPs and DOX-prodrug NPs /siPlk1

After the successful synthesis of C18-N-DOX, self-assembly abilities of C18-N-DOX were evaluated. C18-N-DOX alone could self-assemble in water, but these NPs were easy to aggregate in PBS (pH 7.4). Hence, DSPE-PEG2000, which was approved to be used in clinic by the Food and Drug Administration (FDA), was added to stabilize NPs by steric hindrance. C18-N-DOX together with DSPE-PEG2000 self-assembled into DOX-prodrug NPs. As shown in Fig. 2A, DOX-prodrug NPs, which constructed with C18-N-DOX: DSPE-PEG2000 molar ratio of 26:1, 12:1 and 7:1, had no obvious difference in size, but which constructed with C18-N-DOX: DSPE-PEG2000 molar ratio of 26:1 and 12:1 were not stable in PBS (pH 7.4). DOX-prodrug NPs, which constructed with C18-N-DOX: DSPE-PEG2000 molar ratio of 4.5:1 and 3:1, had large sizes and wide polydispersity index (PDI). Therefore, DOX-prodrug NPs, which constructed with C18-N-DOX: DSPE-PEG2000 molar ratio of 7:1, were chosen as our following experiment conditions.

Many papers reported that the CG pairs of the DNA motif provided loading sites for DOX.<sup>36,37</sup> They demonstrated this by measuring the fluorescence intensity of DOX. When a fixed concentration of DOX was incubated with an increasing molar ration of the DNA, the fluorescence intensity of DOX was decreased due to the initiation of förster resonance energy transfer between DOX molecules when loaded into DNA.<sup>38</sup> siRNA with double strands contains CG base pairs, and it is speculated that DOX may load into siRNA. To examine whether the DOX-prodrug NPs have another way to bind siRNA, the fluorescence spectra of the free DOX and DOX-prodrug NPs were measured. As shown in Fig. S2, the intensity of fluorescence of DOX was decreased, suggesting that free DOX intercalated into siRNA. As shown in Fig. S3, the intensity fluorescence of C18-N-DOX slight decreased. It was suggested that DOX modified

with C18 inhibited its ability to intercalate in siRNA. Daunomycin and doxorubicin are anthracycline anticancer drug with the same mechanism to kill tumors that bind to DNA and blocks its replication. Daunomycin complexes with DNA through two bonds: one at the chromophore, the other at the amino-sugar. The amino-sugar closes to a sugar-phosphate chain enabling the ionized amino group to interact strongly with the second DNA phosphate.<sup>39</sup> Kinetic studies of daunomycin intercalating in DNA by Richard Lavery and co-workers suggested that the optimal pathway involves initial binding to the minor groove by its amino sugar and an activated process causes the drug to rotate and to partially insert its planar anthraquinone moiety into a wedge formed between two successive base pairs.<sup>40</sup> Our experiment conjugated DOX with C18 by carbamate linkage, which amino group cannot ionize. Therefore, C18-N-DOX may decrease the ability of DOX to intercalate in siRNA, since carbamate bond did not strongly interact with the siRNA phosphate and inhibited the DOX initial binding to siRNA. To further confirm this, the DOX-prodrug NPs were prepared in pH 7.4 PBS, in order to avoid the effect of cationic charges. The fluorescence spectra assay (Fig. S4) and the gel electrophoresis assay (Fig. 2B (a)) indicated that the ability of DOX-prodrug NPs binding siRNA in pH 7.4 PBS was very weak. It has been reported that tertiary amines possess positive charge density in low pH and have ability of complexing siRNA.<sup>26-30</sup> DOX-prodrug NPs/siRNA were made using previous reported method with some modification.<sup>31</sup> As shown in Fig. 2B (b), we found that DOX-prodrug NPs constructed with C18-N-DOX: DSPE-PEG2000 molar ratio of 7:1 had strong abilities of binding siRNA in citrate buffer (pH 3), which completely complexed siRNA at NPs/siRNA weight ratio of 21:1, leading to no free siRNA band in the gel. These results coincided with the previous report that all primary amines and tertiary amines are protonated (pH < 4).<sup>26</sup> These results showed that DOX-prodrug NPs mainly complexed siRNA through

electrostatic interaction. The equivalent DOX loading efficiency of DOX-prodrug NPs was 39.8%. The DOX-prodrug NPs and the DOX-prodrug NPs/siRNA were prepared and characterized by TEM. As shown in Fig. 2C (a), DOX-prodrug NPs were spherical micelles with unimodal size distribution by TEM. The Cryo-TEM image of DOX-prodrug NPs also confirmed DOX-prodrug NPs were spherical micelles (Fig. S5). Compared with the morphology of DOX-prodrug NPs, the DOX-prodrug NPs/siRNA had high electronic intensity in periphery by TEM, suggested that siRNAs were complexed at the surface of DOX-prodrug NPs through electrostatic interaction (Fig. 2C (b)). The resulting DOX-prodrug NPs/siRNA had a mean diameter of approximately 100 nm as the similar size as DOX-prodrug NPs. However, the zeta potential of DOX-prodrug NPs (-1.2 mV) and DOX-prodrug NPs/siRNA (-7.9 mV) in PBS (pH 7.4) had some different values, indicating that DOX-prodrug NPs could complex with the siRNA. The stability of DOX-prodrug NPs/siRNA was investigated in DMEM containing 10% FBS. As shown in Fig. 2D, for 40 h incubation the size of DOX-prodrug NPs/siRNA slightly increased from 100.2 nm to 121.2 nm. This result suggested that DOX-prodrug NPs/siRNA had better colloidal stability in 10% FBS. These findings are important because the slight negative surface charge will enhance the colloidal stability and prolong the NPs residence time in the body, as it prevents NPs from protein adsorption and aggregation.<sup>41</sup> Incubation of DOX-prodrug NPs in PBS (pH 7.4) showed the evidenced for slow releasing of DOX (Fig. S6). After 4 days of incubation, about 12.5% of the total drug content was liberated from DOX-prodrug NPs. This suggested that DOX-prodrug NPs enhanced stability in physiological environment. The sustained release of DOX-prodrug NPs is likely due to retarded hydrolysis and drug diffusion within the hydrophobic core.<sup>42</sup>

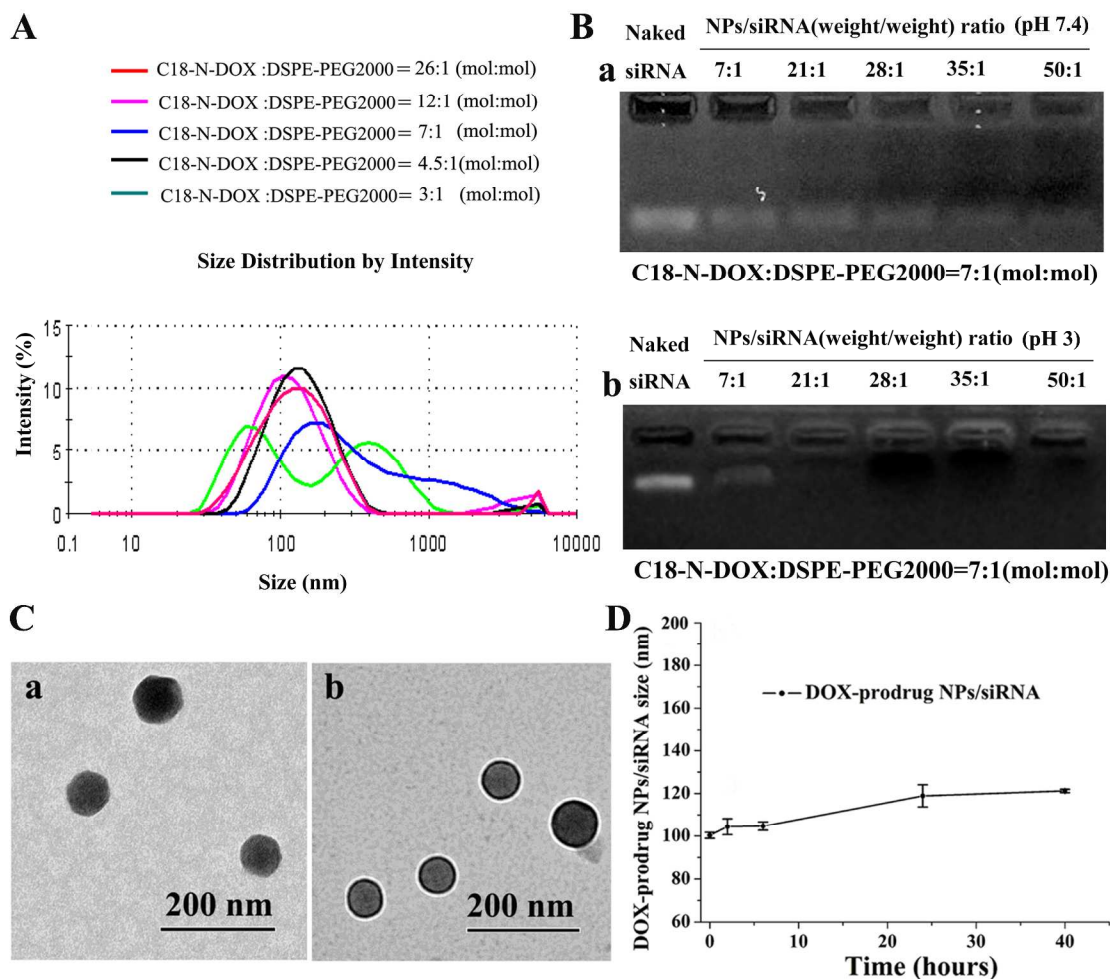


**Fig. 2** A) The size distribution of DOX-prodrug NPs constructed with different molar ratio of C18-N-DOX: DSPE-PEG2000. B) Gel retardation assay of complexation efficiency of siRNA at various NPs/siRNA weight ratios. a. The NPs were prepared and complexed with siRNA in pH 7.4 PBS. b. The NPs were complexed siRNA in pH 3 citrate buffer. C) a. The TEM image of DOX-prodrug NPs. b. The TEM image of DOX-prodrug NPs/siRNA. (Scale bar: 200 nm). D) The stability of DOX-prodrug NPs/siRNA in DMEM with 10% FBS.

### ***In vitro* analysis of delivery of siRNA into tumor cells**

Previous reports indicated that DOX was conjugated with C18 by carbamate bond, which liable to acid-catalyzed hydrolysis to release free DOX in the cells.<sup>43,44</sup> To investigate the intracellular drug release, DOX fluorescence in *HeLa* cells was observed by CLSM. Fig. S7 showed the

absorption spectrum of free DOX as well as C18-N-DOX near 485 nm by using ultraviolet spectrophotometer. So, DOX conjugated with C18-N-OH cannot change the absorbance peak of DOX. As shown in Fig. S8a, when cells were incubated with DOX-prodrug NPs and DOX-prodrug NPs/anticancer siRNA, considerable fluorescence intensity was detected in the mainly cytoplasm within 2 h incubation. However, cellular fluorescence was much higher and part of the DOX molecules were localized in the cell nuclei after 24 h incubation (Fig. S8b). This result suggested that DOX released from C18-N-DOX and entered into cell nuclei to kill tumor cells. DOX localized in the cell nuclei is likely intercalated into DNA strands, thereby showing its toxicity against tumor cells.

To demonstrate the simultaneous delivery, DOX-prodrug NPs/Cy5-siRNA containing C18-N-DOX and Cy5-siRNA were prepared as described above. Cells were incubated with DOX-prodrug NPs/Cy5-siRNA for 2 h. Fluorescence-activated cell sorting (FACS) analysis showed that the cells were located only in the double-positive quadrant, indicating the DOX-prodrug NPs indeed delivered siRNAs into the cells (Fig. 3A). Simultaneous delivery was corroborated by CLSM, which showed colocalization of the C18-N-DOX (red) and Cy5-siRNA (green) fluorescence distributed in the cytoplasm (Fig. 3B). These results indicated that the DOX-prodrug NPs delivered siRNA into the cells.

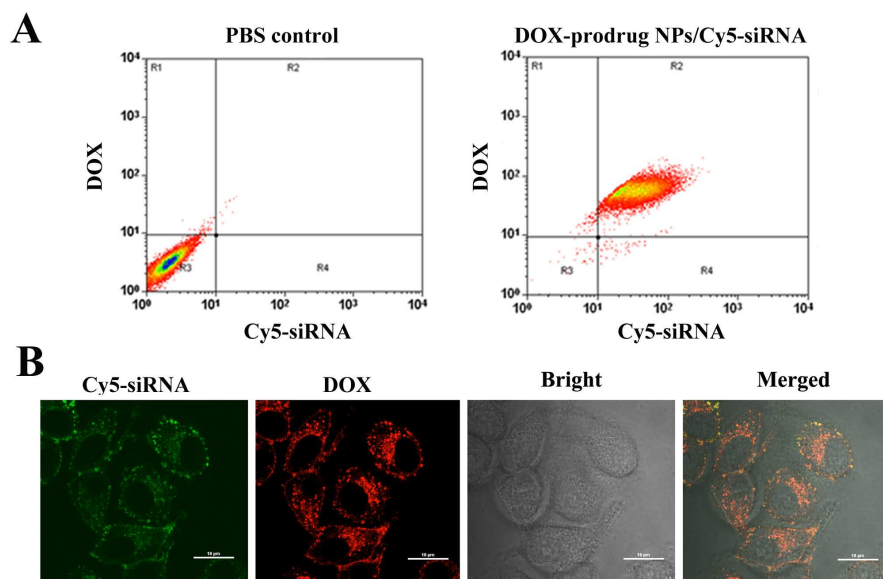


**Fig. 3** A) Cellular uptake of DOX-prodrug NPs/Cy5-siRNA for 2 h as analyzed by FACS. B) CLSM image of intracellular distribution of DOX-prodrug NPs/Cy5-siRNA in *HeLa* cell after incubation of 2 h.. Scale bar: 20  $\mu\text{m}$ . DOX-prodrug NPs had DOX auto-fluorescence (red) and Cy5-siRNA stained as green. Both FACS and CLSM analyses were performed after incubating DOX-prodrug NPs/Cy5-siRNA with *HeLa* cells at NPs/siRNA weight ratio of 21:1.

### ***In Vitro* Gene Silencing Ability**

The ability of DOX-prodrug NPs binding siLuc to silence gene expression was performed. The siLucs were complexed with DOX-prodrug NPs to transfect *HeLa*-Luci cells. As shown in Fig. 4A, DOX-prodrug NPs/siLuc efficiently downregulated the Luc expression. Next, the siPlk1 were chosen as model siRNA drug to kill tumor. Since siPlk1 could downregulate Plk1 protein expression and prolong the cells in  $G_2/M$  phase arrest, which promoted cell apoptosis and induce cell death, it was used as a model siRNA drug in our work.<sup>45-47</sup> In this study, the *HeLa* cell line as an *in vitro* model system was used to test DOX-prodrug NPs/siPlk1 for knockdown the expression of Plk1, due to Plk1 over-expressed in *HeLa* tumor types. Herein, the ability of downregulating therapeutic target mRNA level by siPlk1 delivered by DOX-prodrug NPs was



assessed by RT-PCR. As shown in Fig. 4B, DOX-prodrug NPs complexed with 125 nM siPlk1 could significantly silence Plk1 gene expression in *HeLa* cells, leading to approximately 67.2% knockdown of Plk1 mRNA, reaching a similar level to that of Lipofectamin2000 (Lipo/siPlk1) (68.8% of the PBS control). However, negative controls including treatments with PBS, free siPlk1 and DOX-prodrug NPs/nonsense siRNA showed no knockdown efficiency. Downregulation of Plk1 mRNA expression was subsequently accompanied by decreased Plk1 protein expression. Following transfection with DOX-prodrug NPs/siPlk1 and DOX-prodrug NPs/nonsense siRNA, Plk1 protein expression levels were detected by Western blot analysis. DOX-prodrug NPs/siPlk1 significantly enhanced silencing of Plk1 protein expression compared with DOX-prodrug NPs/nonsense siRNA (Fig. 4C and D). The free siPlk1 and DOX-prodrug NPs/nonsense siRNA did not downregulate Plk1 protein expression in *HeLa* cells. These findings indicated that DOX-prodrug NPs could be exploited as an efficient delivery system for therapeutic siRNAs.

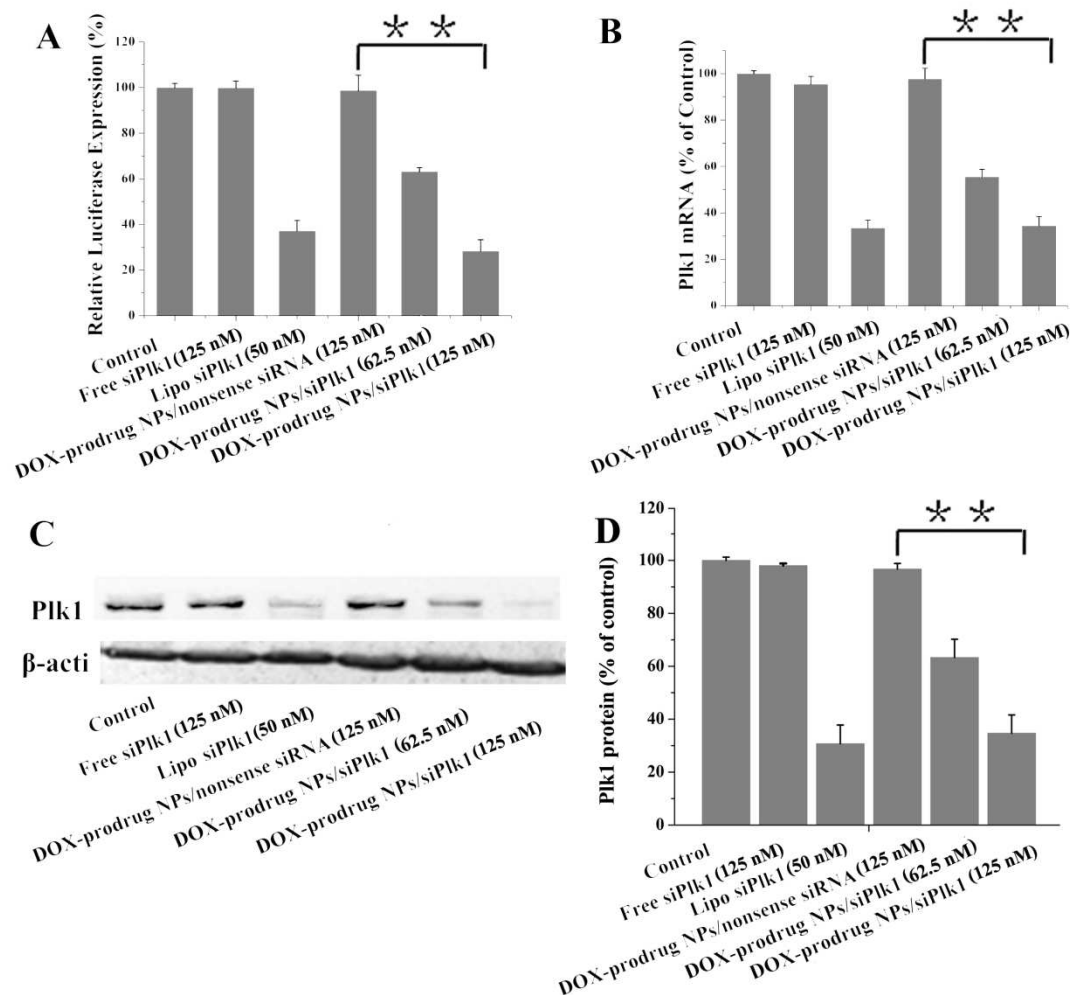


**Fig. 4** A) Knockdown the expression of luciferase. B) Knockdown the expression of Plk1 mRNA. C) The expression level of Plk1 protein. *HeLa* cells are incubated with DOX-prodrug NPs/siPlk1 for 48 h. Data are presented as a mean  $\pm$  SD,  $n = 3$ ,  $**p < 0.01$ . *HeLa* cells are transfected with free siPlk1 and DOX-prodrug NPs/nonsense siRNA with 125 nM siRNA doses. The concentration of siPlk1 with Lipofectamine 2000 (Lipo/siPlk1) is 50 nM. *HeLa* cells are transfected with DOX-prodrug NPs with siPlk1 doses 62.5 nM and 125 nM, respectively.

### Inhibition of Cancer Cell Proliferation *In Vitro*

As in the previous design, the DOX-prodrug NPs could deliver siRNAs. SiPlk1 could inhibit cell proliferation through inducing cell apoptosis. From the above RT-PCR and Western blot analysis, DOX-prodrug NPs/siPlk1 had the most efficient siPlk1 silencing ability. In follow-up

experiments, the cooperation effects were assessed *in vitro* by IC<sub>50</sub>. MTT assay was employed to assess the antitumor activities of these NPs *in vitro*. The MTT data showed that DOX-prodrug NPs/siPlk1 could obviously inhibit the proliferation of the *HeLa* cells, as shown by a 4-fold decrease in IC<sub>50</sub> values from the nonsense siRNA control (IC<sub>50</sub> = 1.31 μM) to the combination siPlk1 with DOX-prodrug NPs treatment (IC<sub>50</sub> = 0.32 μM) at 48 h (Fig. 5). Altogether, these data indicated that the DOX-prodrug NPs/siPlk1 exerted the stronger combined inhibiting effect on *HeLa* cells growth.

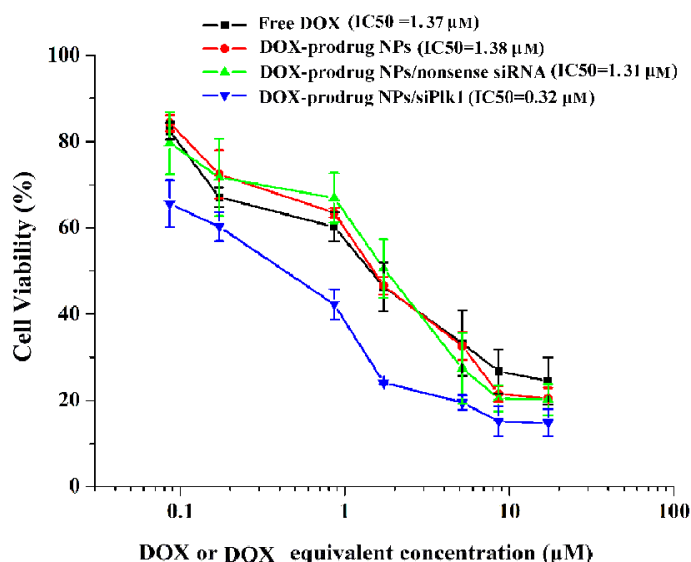


**Fig. 5** Cell viability study of *HeLa* cells incubated with free DOX, DOX-prodrug NPs, DOX-prodrug NPs/nonsense siRNA and DOX-prodrug NPs/siPlk1 with different DOX or DOX equivalent concentration. DOX-prodrug NPs/nonsense siRNA and DOX-prodrug NPs/siPlk1 with NPs/siRNA weight ratio 21:1. Data represent mean  $\pm$  SD, n = 3.

### Tumor Growth Suppression *In Vivo*

To examine the combined effects of DOX and siPlk1, tumor growth inhibitory effects were studied *in vivo*. To inhibit the tumor growth by DOX-prodrug NPs/siPlk1, DOX-prodrug NPs/siPlk1 should efficiently target the tumor sites. Firstly, we used DOX-prodrug NPs to bind

Cy5-siRNA which is used as an *in vivo* tracer in living organisms. PBS (pH 7.4, 200  $\mu$ L), free Cy5-siRNA (at siRNA dose of 1 mg kg<sup>-1</sup>) and DOX-prodrug NPs/Cy5-siRNA (at siRNA dose of 1 mg kg<sup>-1</sup>) were injected via tail vein in *HeLa*-bearing BALB/c nude mice. The organs of the mice were collected and observed by an *in vivo* imaging system. As shown in Fig. 6A, the Cy5-siRNA fluorescence was detected at the tumor site in mice injected with DOX-prodrug NPs/Cy5-siRNA, demonstrating the accumulation of DOX-prodrug NPs/Cy5-siRNA in tumor tissues by the enhanced permeability and retention (EPR) effect. Meanwhile, a strong signals for both DOX-prodrug NPs/Cy5-siRNA and free Cy5-siRNA was observed in the kidney, reflecting renal clearance of NPs and free siRNA. This result coincided with the previous report that free siRNA molecules into the bloodstream are subjected to rapid clearance from the blood through liver accumulation and renal filtration.<sup>48</sup> A high intensity of DOX-prodrug NPs/Cy5-siRNA in the liver was observed, implicating that intravenously injected particles were scavenged and cleared from circulation by the reticuloendothelial system.<sup>49</sup> The tumor distribution of DOX-prodrug NPs/Cy5-siRNA was confirmed by frozen tumor tissue section observed by CLSM. As shown in Fig. 6B, Cy5-siRNA fluorescence (green) and DOX fluorescence (red) were observed in tumor tissue. Altogether, these data indicated that DOX-prodrug NPs could simultaneously deliver into the tumor site by EPR effect.

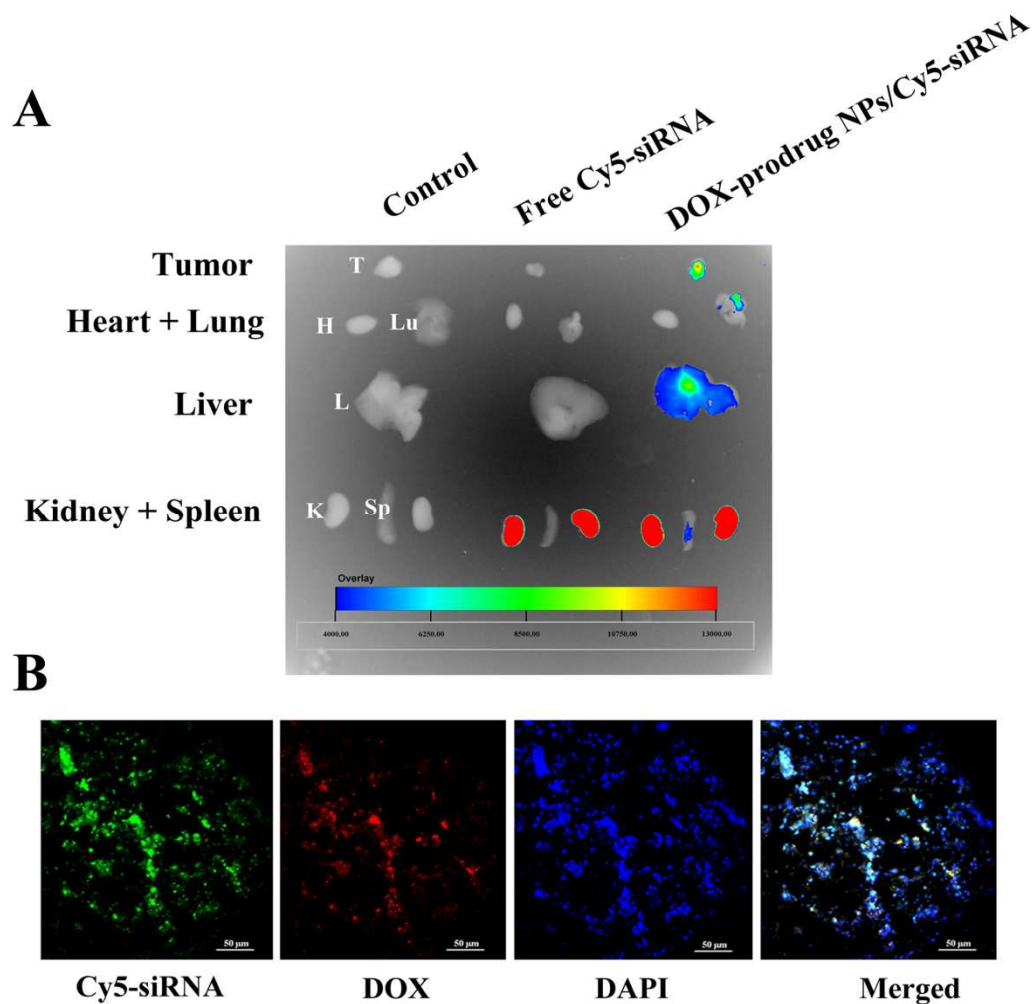


**Fig. 6** A) *In vivo* Cy5-siRNA distribution in the tumor and organs at 24 h after intravenous injection of Cy5-siRNA ( $1 \text{ mg kg}^{-1}$ ) to mice with DOX-prodrug NPs. a. Control, b. Free Cy5-siRNA, c. DOX-prodrug NPs/Cy5-siRNA. Tumor (T), Heart (H), Lung (Lu), Liver (L), Kidney (K) and Spleen (Sp). B) CLSM images show the distribution of DOX and Cy5-siRNA in tumor following intravenous injection of DOX-prodrug NPs/Cy5-siRNA. DOX (red), Cy5-siRNA (green) and cell nuclei are stained with DAPI (blue). Scale bar: 50  $\mu\text{m}$ .

Due to DOX self-fluorescence, DOX-prodrug NPs, DOX-prodrug NPs/siPlk1 and free DOX were used to evaluate the tissue distribution. The tissue distribution of DOX-prodrug NPs/siPlk1, DOX-prodrug NPs and free DOX were examined 12 h after the intravenous injection

in ICR mice. The organs of the mice were collected and observed by an *in vivo* imaging system. A strong signal for both DOX-prodrug NPs/siPlk1 and DOX-prodrug NPs was observed in the kidney, reflecting renal clearance of NPs. A higher intensity of DOX-prodrug NPs in the liver was observed than DOX-prodrug NPs/siPlk1, implicating that the liver readily captured DOX-prodrug NPs, which had separated with DOX during blood circulation (Fig. 7A and Fig. 7B). The plasma DOX concentration was measured as a function of time post-injection. To measure the retention time of DOX in blood via NPs delivery, free DOX, DOX-prodrug NPs and DOX-prodrug NPs/siPlk1 were injected to mice with the same concentration of  $4.1 \text{ mg kg}^{-1}$  DOX. One- and noncompartment pharmacokinetic model was used to fit the plasma concentration-time profiles (Fig. 7C). The DOX-prodrug NPs/siPlk1 delivery extended the plasma half-time of DOX to  $\approx 12.5 \text{ h}$  as compared with free DOX ( $\approx 0.18 \text{ h}$ ). The DOX-prodrug NPs delivery extended the plasma half-time of DOX to  $\approx 8.2 \text{ h}$ . The tumor distribution of DOX-prodrug NPs/siPlk1, DOX-prodrug NPs and free DOX were observed 12 h after the intravenous injection in *HeLa*-bearing BALB/c nude mice. As shown in Fig. 7D, the DOX fluorescence was detected at the tumor in mice injected with DOX-prodrug NPs/siPlk1, DOX-prodrug NPs and the free DOX. However, the strongest DOX fluorescence was observed in the tumor, which injected with DOX-prodrug NPs/siPlk1, indicating that the more accumulation of DOX than DOX-prodrug NPs and free DOX in the tumor tissues. Taken together, these findings demonstrated that DOX-prodrug NPs/siPlk1 were able to successfully deliver DOX and siPlk1 to target tumor *in vivo* and could extensively prolong the retention time of DOX in blood. It is speculated that the negative surface charge of DOX-prodrug NPs/siPlk1 prevented nonspecific protein adsorption and aggregation of DOX-prodrug NPs/siPlk1 *in vivo*, thus more DOX-prodrug NPs/siPlk1 accumulated in the tumor through the EPR effect and DOX-prodrug NPs/siPlk1 had long retention time of DOX. Long-

circulating DOX-prodrug NPs/siPlk1 provided more chance for siPlk1-PCNPs/DOX accumulation in the tumor sites.

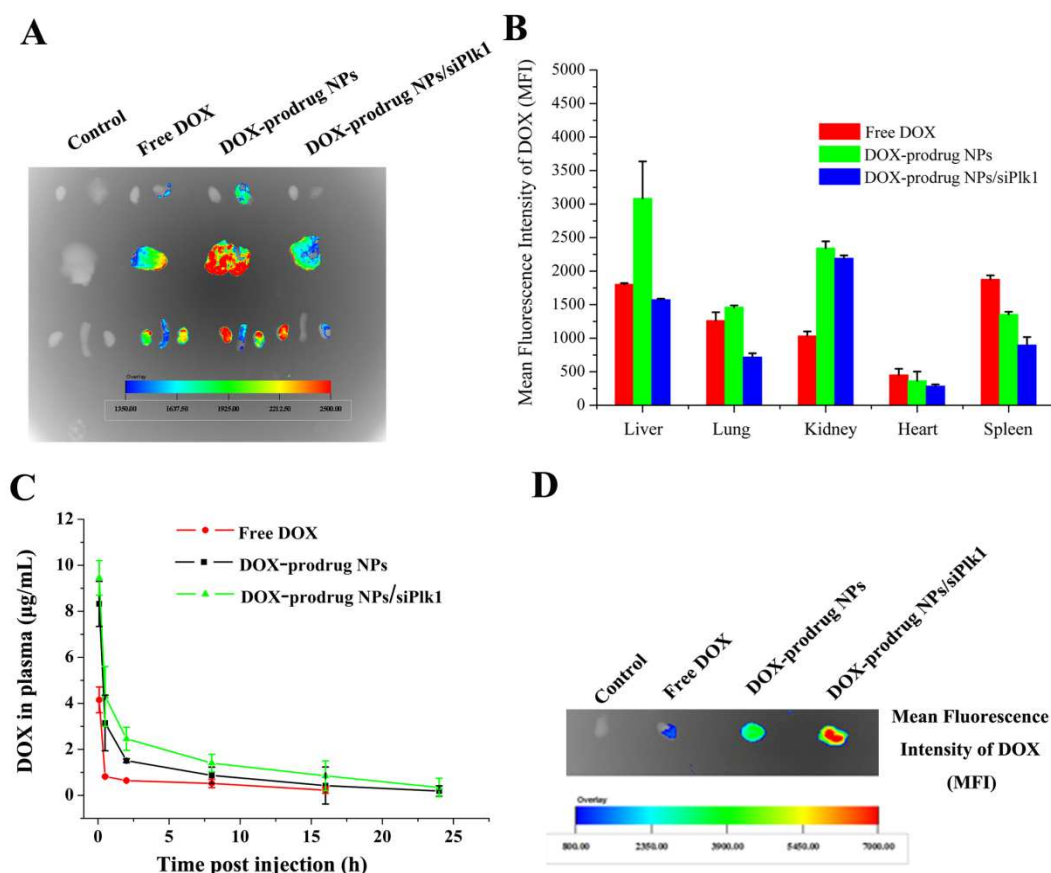


**Figure 7.** *In vivo* DOX distribution in the organs after intravenous injection to mice with free DOX, DOX-prodrug NPs and DOX-prodrug NPs/siPlk1. A) Fluorescent image of tissues distribution of free DOX, DOX-prodrug NPs and DOX-prodrug NPs/siPlk1 at 12 hour-post injection. Free DOX, DOX-prodrug NPs and DOX-prodrug NPs/siPlk1 were intravenously injected to ICR mice. (DOX concentration of  $4.1 \text{ mg kg}^{-1}$ ). B) Quantitative analysis of DOX in tissue. C) Blood retention kinetics of free DOX, siPlk1-NPs/DOX and siPlk1-PCNPs/DOX in ICR mice. (DOX concentration of  $4.1 \text{ mg kg}^{-1}$ ). Means  $\pm$  SD,  $n = 4$ . D) Tumor distribution of DOX at 12 hour-post injection. Free DOX, DOX-prodrug NPs and DOX-prodrug NPs/siPlk1 were intravenously injected to *HeLa*-bearing BALA/c nude mice. (DOX concentration of  $4.1 \text{ mg kg}^{-1}$ ).

Next, we examined the antitumor growth effect of DOX-prodrug NPs/siPlk1 after accumulation in the tumor site. Free siPlk1, DOX-prodrug NPs/nonsense siRNA and DOX-

prodrug NPs/siPlk1 were intravenously injected at days 0, 2, 4 and 6. As shown in Fig. 8A, complete tumor regression was observed in DOX-prodrug NPs/siPlk1 group, which inhibited the average tumor volume by 5.1-fold compared to the PBS control. Partial tumor regression was seen in free DOX and DOX-prodrug NPs/nonsense siRNA group, which suppressed the tumor volume by 1.6-fold and 2.2-fold, respectively, compared with the PBS control. Moreover, compared with free DOX, DOX-prodrug NPs/nonsense siRNA had high antitumor activity, due to DOX-prodrug NPs/nonsense siRNA delivery more DOX to tumor than free DOX, which confirmed by distribution of DOX fluorescence in tumor tissue (Fig. 7D). From this result, we found that siPlk1 enhanced DOX antitumor therapy through silencing of Plk1 gene expression. The tumor continued to grow, and no obviously inhibition of tumor growth was observed when *HeLa*-bearing mice injected free siPlk1. Free siRNA molecules were subjected to rapid clearance from the blood through liver accumulation and renal filtration.<sup>48</sup> Therefore, free siPlk1 had no obvious decrease in the tumor volume. As shown in Fig. 8B, no obvious body weight loss was observed for the mice treated with DOX-prodrug NPs/siPlk1 or DOX-prodrug NPs/nonsense siRNA. A slight body weight loss was observed in the mice group treatment with free DOX. Altogether, these data indicated that reduced toxic side effects of the DOX-prodrug NPs. To demonstrate that inhibited tumor growth by DOX-prodrug NPs/siPlk1 was related to Plk1 downregulation in tumor cells, the tumors were excised 24 h after the last injection. Plk1 mRNA expression was analyzed by RT-PCR. Xenografts from mice treated by DOX-prodrug NPs/siPlk1 containing siPlk1 reduced Plk1 mRNA levels ( $\approx 67.4\%$  of the PBS control). Based on the RT-PCR data (Fig. 8C), *HeLa*-bearing mice injected with free siPlk1 and DOX-prodrug NPs/nonsense siRNA did not downregulate the Plk1 mRNA level. Tumor Plk1 protein expression was analyzed by Western blot analyses. Western blot analyses of Plk1 protein levels



in tumor tissues (Fig. 8D) revealed a significant reduction in Plk1 protein levels when the mice were treated with DOX-prodrug NPs/siPlk1. In contrast, there was no decrease in Plk1 protein levels after treatments with free siPlk1 and DOX-prodrug NPs/nonsense siRNA, compared to the treatment with PBS.

DOX and siPlk1 were proven to inhibit the growth of cancer by inducing apoptosis on tumor. To examine whether cell apoptosis was induced the decrease of the tumor volume, the tumor tissues were collected for TUNEL analyses 24 h after the last injection. The combined therapy significantly increased TUNEL-positive tumor cells, compared with free siPlk1 and DOX-prodrug NPs/nonsense siRNA treatment (Fig. 8E). Notably, DOX-prodrug NPs/siPlk1 injected achieved the highest cell apoptosis and remarkably decreased the percentage of proliferating tumor cells in the studied tumor tissue section (Fig. 8E (e)). These data indicated that DOX-prodrug NPs/siPlk1 showed enhanced efficiency for tumor treatments by inducing apoptosis and prohibited the proliferation of tumor cells.

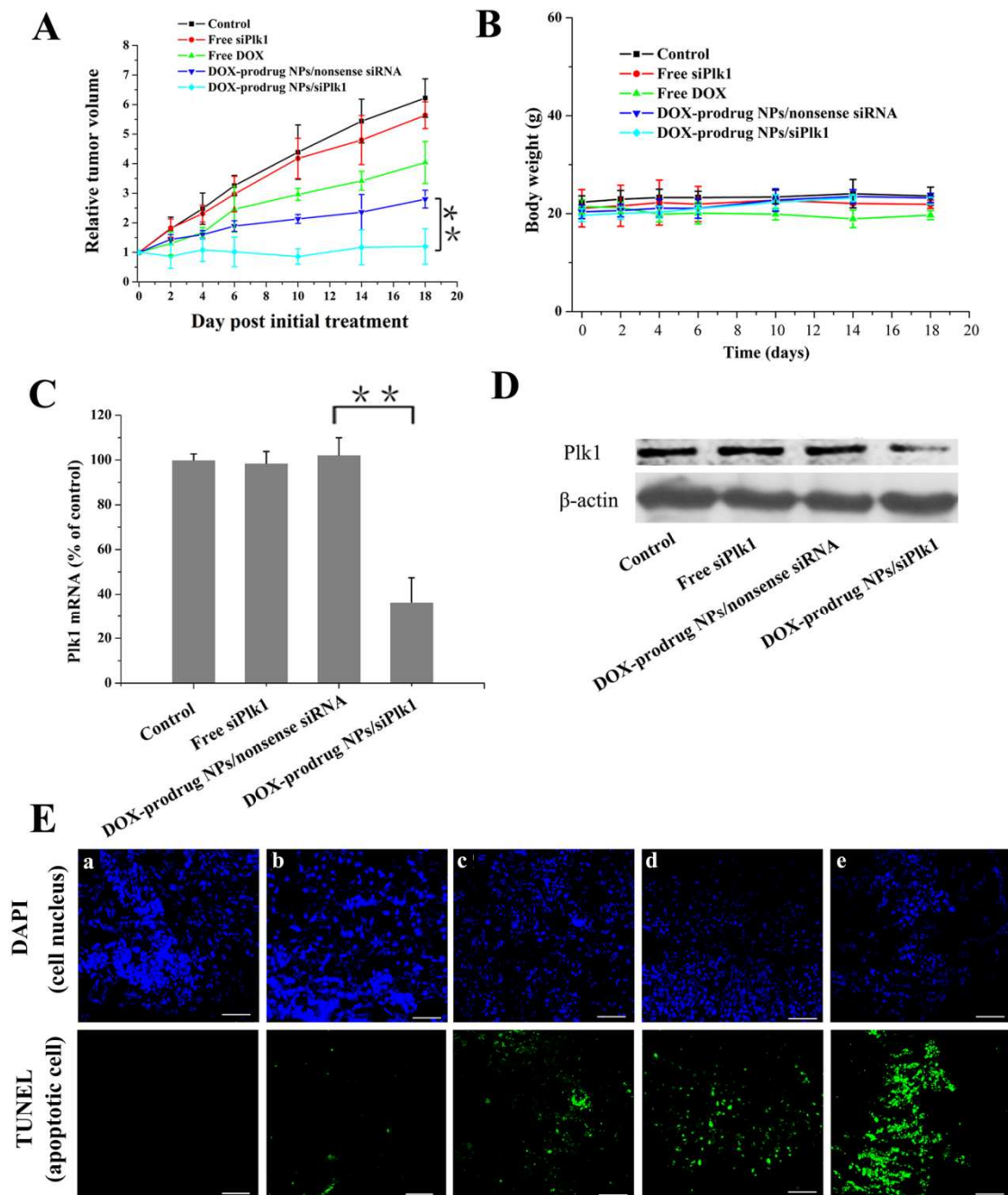


**Figure 8.** A) Antitumor efficacies *in vivo* after tail vein injection of PBS, free siPlk1, free DOX, DOX-prodrug NPs/nonsense siRNA and DOX-prodrug NPs/siPlk1 on *HeLa*-bearing female BALB/c nude mice. B) Changes in body weight, C) RT-PCR analyses of Plk1 mRNA in tumor after injections of different formulations. D) Western blot analyses of Plk1 protein in tumor after injections of different formulations. Each formulation was administered on days 0, 2, 4, and 6 by tail vein injection at a dose of  $4.1 \text{ mg kg}^{-1}$  DOX equivalent and at a dose

of  $0.5 \text{ mg kg}^{-1}$  siRNA. The tumor tissues were collected for RT-PCR and Western blot analyses 24 h after the last injection. Means  $\pm$  SD,  $n=4$ ,  $**p<0.01$ . E) *In vivo* TUNEL analyses of tumor sections from mice receiving different formulations. In TUNEL analysis, green stains indicated apoptotic, DAPI was used to stain cell nucleus (blue). a) PBS, b) free siPlk1, c) free DOX, d) DOX-prodrug NPs/nonsense siRNA, and e) DOX-prodrug NPs/siPlk1.

DOX is a highly effective and widely used chemotherapeutic drug to cure various types of cancer. Its effectiveness is limited by its cardiac toxicity. In order to further evaluate the cardiotoxicity of DOX and DOX-prodrug NPs treatment, the histological analysis of the cardiac tissues were tested. As shown in Fig. 9, histological examinations did not show any myocardial lesions in the group of mice treated with free DOX, DOX-prodrug NPs, DOX-prodrug NPs/nonsense siRNA and DOX-prodrug NPs/siPlk1, suggesting that the treatment with free DOX, DOX-prodrug NPs, DOX-prodrug NPs/nonsense siRNA and DOX-prodrug NPs/siPlk1 at the experimental dosage did not damage the heart of the mice during the experimental period.

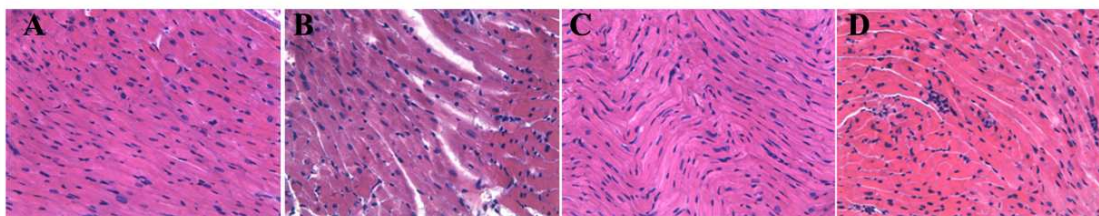


**Fig. 9** Histopathology of H & E-stained myocardial tissue from *HeLa*-bearing nude mice treatment with different formulations. All images were analyzed by microscopy at  $400 \times$  magnification. A) PBS, B) free DOX, C) DOX-prodrug NPs/nonsense siRNA, and D) DOX-prodrug NPs/siPlk1.

## Conclusions

In summary, we developed DOX-prodrug NPs for siRNA delivery. The conjugated DOX and pH-responsive tertiary amine with DOX-prodrug NPs could successfully enhance the DOX loading efficiency, decrease the inert materials to embed DOX and reduce the cationic charge

densities on the NPs surface. We have demonstrated that the DOX-prodrug NPs significantly downregulated the expression levels of target genes (siPlk1) *in vitro* and *in vivo*. In animal experiment, the DOX-prodrug NPs/siPlk1 significantly inhibited tumor growth in a combined manner. This finding suggested that the DOX-prodrug NPs had the potential for delivery siRNA and provided a promising nanomedicine approach for cancer treatment.

### Acknowledgments

This work was financially supported by National Natural Science Foundation of China (Grants NO. 21304099, 51203162, 51103159, 51373177), the National High Technology Research and Development Program (Grants NO. 2014AA020708, 2012AA022703, 2012AA020804), Instrument Developing Project of the Chinese Academy of Sciences (Grant No. YZ201253, YZ201313), Open Funding Project of the National Key Laboratory of Biochemical Engineering (Grant No. Y22504A169). “Strategic Priority Research Program” of the Chinese Academy of Sciences, Grant No. XDA09030301-3.

### Notes and references

- 1 A. Jemal, F. Bray, M. M. Center, J. Ferlay, E. Ward, D. Forman, *CA Cancer J Clin*, 2011, 61, 69–90.
- 2 M. Khan, Z. Y. Ong, N. Wiradharma, A. B. Attia, Y. Y. Yang, *Adv. Healthc. Mater.*, 2012, 1, 373–392.
- 3 H. H. Duong, L. Y. Yung, *Int J Pharm*, 2013, 454, 486–495.
- 4 X. Y. Ke, V. W. Lin Ng, S. J. Gao, Y. W. Tong, J. L. Hedrick, Y. Y. Yang, *Biomaterials*, 2014, 35, 1096–1108.
- 5 H. Xiao, W. Li, R. Qi, L. Yan, R. Wang, S. Liu, Y. H. Zheng, Z. G. Xie, Y. B. Huang, X. B. Jing, *J Control Release*, 2012, 163, 304–314.

- 6 O. Taratula, A. Kuzmov, M. Shah, O.B. Garbuzenko, T. Minko, *J Control Release*, 2013, 171, 349–357.
- 7 L. Li, W. Gu, J. Chen, W. Chen, Z. P. Xu. *Biomaterials*, 2014, 35, 3331–3339.
- 8 F. Zhao, H. Yin, J. Li. *Biomaterials*, 2014, 35, 1050–1062.
- 9 J. Zhao, Y. Mi, S. S. Feng. *Biomaterials*, 2013, 34, 3411–3421.
- 10 H. L. Liu, Y. Li, A. Mozhi, L. Zhang, Y. L. Liu, X. Xu, J. M. Xing, X. J. Liang, G. H. Ma, J. Yang, X. Zhang, *Biomaterials*, 2014, 35, 6519–6533.
- 11 K. Men, M. L. Gou, Q. F. Guo, X. H. Wang, S. Shi, B. Kan, M. J. Huang, F. Luo, L. J. Chen, X. Zhao, Z. Y. Qian, S. F. Liang, Y. Q. Wei, *J Nanosci Nanotechnol*, 2010, 12, 7958–7964.
- 12 S. Biswas, P. P. Deshpande, G. Navarro, N. S. Dodwadkar, V. P. Torchilin., *Biomaterials*, 2013, 34, 1289–1301.
- 13 A. Baeza, E. Guisasola, E. Ruiz-Hernández, M. Vallet-Regí, *Chem. Mater.*, 2012, 24, 517–524.
- 14 Y. Q. Shen, E. Jin, B. Zhang, C. J. Murphy, M. H. Sui, J. Zhao, J. Wang, J. Tang, M. Fan, K. E. Van, W. J. Murdoch, *J. Am. Chem. Soc.*, 2010, 132, 4259–4265.
- 15 M. Shi, K. Ho, A. Keating, M. S. Shoichet, *Adv. Funct. Mater.*, 2009, 19, 1689–1696.
- 16 P. F. Gou, W. W. Liu, W. W. Mao, J. B. Tang, Y. Q. Shen, M. H. Sui, *J. Mater. Chem.*, 2013, 1, 284–292.
- 17 S. Aroui, S. Brahim, M. D. Waard, A. Kenani, *Biochem. Biophys. Res. Commun.*, 2010, 391, 419–425.
- 18 B. L. Davidson, P. B. McCray Jr, *Nat. Rev. Genet.*, 2011, 12, 329–340.
- 19 J. T. Pento, *Drugs Future*, 2007, 32, 1061–1066.
- 20 Y. Chen, J. J. Wu, L. Huang, *Mol Ther.*, 2010, 18, 828–834.

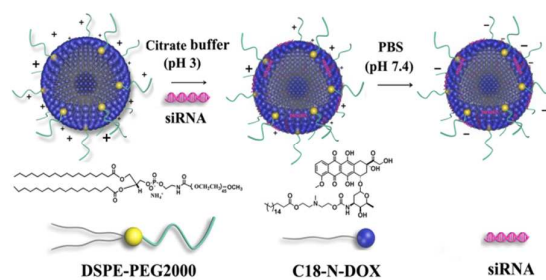
- 21 H. O. Kim, E. Kim, Y. An, J. Choi, E. Jang, E. B. Choi, A. Kukreja, M. H. Kim, B. Kang, D. J. Kim, J. S. Suh, Y. M. Huh, S. Haam, *Macromol Biosci.*, 2013, 13, 745–754.
- 22 J. M. Li, Y. Y. Wang, M. X. Zhao, C. P. Tan, Y. Q. Li, X. Y. Le, L. N. Ji, Z. W. Mao, *Biomaterials.*, 2012, 33, 2780–2790.
- 23 X. B. Xiong, A. Lavasanifar, *ACS Nano*, 2011, 5, 5202–5213.
- 24 S. Zou, N. Cao, D. Cheng, R. Zheng, J. Wang, K. Zhu, X. Shuai. *Int J Nanomed.*, 2012, 7, 3823–3835.
- 25 N. Cao, D. Cheng, S. Y. Zou, H. Ai, J. M. Gao, X. T. Shuai, *Biomaterials*, 2011, 32, 2222–2232.
- 26 P. K. Maiti, T. Cagin, S. T. Lin, W. A. Goddard, *Macromolecules*, 2005, 38, 979–991.
- 27 S. C. Semple, A. Akinc, J. Chen, A. P. Sandhu, B. L. Mui, C. K. Cho, D. W. Y. Sah, D. Stebbing, E. J. Crosley, E. Yaworski, I. M. Hafez, J. R. Dorkin, J. Qin, K. Lam, K. G. Rajeev, K. F. Wong, L. B. Jeffs, L. Nechev, M. L. Eisenhardt, M. Jayaraman, M. Kazem, M. A. Maier, M. Srinivasulu, M. J. Weinstein, Q. M. Chen, R. Alvarez, S. A. Barros, S. De, S. K. Klimuk, T. Borland, V. Kosovrasti, W. L. Cantley, Y. K. Tam, M. Manoharan, M. A. Ciufolini, M. A. Tracy, A. de Fougères, I. MacLachlan, P. R. Cullis, T. D. Madden, M. J. Hope, *Nat Biotechnol*, 2010, 28, 172–176.
- 28 K. T. Love, K. P. Mahon, C. G. Levins, K. A. Whitehead, W. Querbes, J. R. Dorkin, J. Qin, W. Cantley, L. L. Qin, T. Racie, M. Frank-Kamenetsky, K. N. Yip, R. Alvarez, D. W. Sah, A. de Fougères, K. Fitzgerald, V. Kotliansky, A. Akinc, R. Langer, D. G. Anderson, *Proc Natl Acad Sci USA*, 2010, 107, 1864–1869.
- 29 Y. Liu, L. Huang. *Mol Ther.*, 2010, 18, 669–670.

- 30 Y. Sato, H. Hatakeyama, Y. Sakurai, M. Hyodo, H. Akita, H. Harashima, *J Control Release*, 2012, 163, 267–276.
- 31 T. P. Prakash, W. F. Lima, H. M. Murray, S. Elbashir, W. Cantley, D. Foster, *Acs Chem. Biol.*, 2013, 8, 1402-1406.
- 32 D. Nicolas, D. Fabienne, P. Vincent, S. Jean-Marc, B. Olivier, S. L. Cécile, H. Stephanie, S. S. Ulrich, G. Jean-François, M. B. Jacqueline, and P. Véronique, *Bioconjug Chem.*, 2014, 25, 72–81.
- 33 T. M. Sun, J. Z. Du, Y. D. Yao, C. Q. Mao, S. Dou, S. Y. Huang, P. Z. Zhang, K. W. Leong, E. W. Song, J. Wang, *ACS Nano*, 2011, 5, 1483–1494.
- 34 S. Y. Lee, S. Kim, J. Y. Tyler, K. Park, J. X. Cheng, *Biomaterials*, 2013, 34, 552–561.
- 35 H. Cabral, Y. Matsumoto, K. Mizuno, Q. Chen, M. Murakami, M. Kimura, Y. Terada, M. R. Kano, K. Miyazono, M. Uesaka, N. Nishiyama, K. Kataoka, *Nat Nanotechnol*, 2011, 6, 815–823.
- 36 Z. Y. Xiao, C. W. Ji, J. J. Shi, E. M. Pridgen, J. Frieder, J. Wu, O.C. Farokhzad, *Angew. Chem. Int. Ed.*, 2012, 51, 11853–11857.
- 37 R. Mo, T. Y. Jiang, Z. Gu, *Angew. Chem. Int. Ed.*, 2014, 53, 5815–5820.
- 38 B. Doughty, Y. Rao, S. W. Kazer, S. J. J. Kwok, N. J. Turro, K. B. Eisenthal, *J. Phys. Chem. B*, 2013, 117, 15285-15289.
- 39 E. Calendi, A. Di Marco, M. Reggiani, B. Scarpinato, L. Valentini, *Biophys. Acta*, 1965, 103, 25.
- 40 M. Wilhelm, A. Mukherjee, B. Bouvier, K. Zakrzewska, J. T. Hynes, R. Lavery, *J. Am. Chem. Soc.*, 2012, 134, 8588-8596.

- 41 A. Vanessa, P. H. Adriana, L. E. Magda, T. L. Madeline, R. Carlos, *J Nanopart Res*, 2013, 15, 1874–1888.
- 42 F. X. Zhan, W. Chen, Z. J. Wang, W. T. Lu, R. Cheng, C. Deng, F. Meng, H. Liu, Z. Zhong, *Biomacromolecules*, 2011, 12, 3612–3620.
- 43 C. C. Lee, E. R. Gillies, M. E. Fox, S. J. Guillaudeu, J. M. Frechet, E. E. Dy, F. C. Szoka, *Proc. Natl. Acad. Sci.*, 2006, 103, 16649–16654.
- 44 H. S. Yoo, T. G. Park. *J Control Release*, 2001, 70, 63–70.
- 45 F. A. Barr, H. H. Sillje, E. A. Nigg, *Mol. Cell Biol.*, 2004, 5, 429–440.
- 46 Liu, X.; Erikson, R. L. *PNAS.*, 2003, 100, 5789–5794.
- 47 K. Strebhardt, *Nat Rev Drug Discov.*, 2010, 9, 643–U24.
- 48 Y. Y. Huang, J. M. Hong, S. Q. Zheng, Y. Ding, S. T. Guo, H. Y. Zhang, X. Q. Zhang, Q. Du, Z. C. Liang. *Mol. Ther.*, 2011, 19, 381–385.
- 49 H. Amir, P. W. Faraji, *Bioorg. Med. Chem.*, 2009, 17, 2950–2962.



A table of contents entry



The DOX-prodrug NPs can complex siRNA in pH 3 citrate buffer and have slight negative charges on the surface of NPs in pH 7.4 PBS.